JOURNAL OF PROPULSION AND POWER
Vol. 15, No. 2, March–April 1999

Flow and Heat Transfer in a Smooth U-Duct with and without Rotation

Mark A. Stephens* and Tom I-P. Shih†
Carnegie Mellon University, Pittsburgh, Pennsylvania 15213-3890

This study shows that when computing a compressible flow in a rotating duct of a given geometry and radial distance from the axis of rotation, the inlet Mach number must be specified in addition to the inlet Reynolds number, inlet rotation number, coolant-to-wall temperature ratio, and Prandtl number. This is because the inlet Mach number and other dimensionless parameters collectively fix the rotational speed, which strongly influences centrifugal buoyancy. This study also shows the nature of the three-dimensional flow induced by Coriolis force, centrifugal buoyancy, and a 180-deg bend in a U-shaped square duct with smooth walls for three rotation numbers (0, 0.24, and 0.48), and two Reynolds numbers (2.5×10^4 and 5×10^4). Key flow mechanisms that affect heat transfer are identified. The computed heat transfer coefficient on the leading and trailing faces of the rotating duct compares well with available experimental data. This computational study is based on the ensemble-averaged conservation equations of mass, momentum (compressible Navier–Stokes), and energy closed by a k-ω/shear stress transport model of turbulence that can be integrated to the wall; i.e., wall functions were not used. Solutions were generated by using a cell-centered finite volume method on a structured grid based on second-order accurate Roe differencing, and on a diagonalized alternating-direction implicit scheme with local time-stepping and V-cycle multigrid.

Nomenclature

D_h = hydraulic diameter of duct
h = heat transfer coefficient, $q_w/(T_w - T_b)$
k = turbulent kinetic energy
M_i = Mach number, $V_i/\sqrt{\gamma \bar{R} T_i}$
Nu = Nusselt number, hD_h/κ
Nu_s = Nusselt number for smooth duct, $0.021 Re^{0.8} Pr^{0.5}$
q_w = wall heat transfer rate per unit area
$\bar{R}$ = gas constant for air
Re = Reynolds number, $\rho_i V_i D_h/\mu_i$
R_i, R_o = inner and outer radius of 180 deg bend, Fig. 1
Ro = rotation number, $\Omega D_h/V_i$
R_r, R_t = radius from axis of rotation, Fig. 1
T = temperature
T_b = pseudobulk temperature given by Eq. (4a)
u, v, w = x, y, z component of velocity vector relative to duct
V_i = average velocity at duct inlet
X' = distance along duct measured from duct inlet, $x - R_r$
x, y, z = coordinate system rotating with duct with origin on rotation axis, Fig. 1
γ = ratio of specific heats, 1.4
$\Delta\rho/\rho$ = density ratio, $(T_w - T_i)/T_w$
κ = thermal conductivity
μ = dynamic viscosity
ρ = coolant density
Ω = angular speed of duct
ω = dissipation rate of k per unit k

Subscripts
i = coolant conditions at duct inlet
w = wall

Introduction

ADVANCED gas-turbine stages, because of their high-temperature operating conditions, require cooling to maintain structural integrity and acceptable life expectancy. One effective and widely used method of cooling is to bleed lower-temperature air from the compressor and circulate it inside and/or outside of each blade. This air, referred to as coolant, typically enters each blade from its root, and exits from its tip and/or trailing edge. It could also exit from any part of the blade surface for film cooling. While inside the blade, the coolant typically flows through a series of straight ducts with rectangular cross sections connected by 180-deg bends.

The importance of internal cooling has led many investigators to study the flow and heat transfer inside ducts. Several experimental studies on rotating ducts have been reported.[1–15] These investigators measured heat transfer characteristics to study the effects of Reynolds number, rotation number, and a buoyancy parameter that accounts for the coolant-to-wall temperature ratio, rotational speed, and the radial position of the duct relative to the axis of rotation. The effects of duct-cross-section aspect ratio, rib blockage, and nonuniformity in duct wall temperature and heat transfer rate were also studied.

Three key results from the experimental studies are as follows. The first is that the leading and trailing faces of a rotating duct (see Fig. 1) have different heat transfer rates. This is a consequence of the secondary flows induced by the Coriolis force. For radially outward flow in a smooth duct, this secondary flow transports cooler fluid from near the center of the duct toward the trailing face, so that the thermal boundary layer caused by this secondary flow starts there, grows along the two side walls, and ends at the leading face. This causes the heat transfer rate to be higher at the trailing face and lower at the leading face. For radially inward flow, the reverse is true; i.e., the leading face would have the higher heat transfer

Presented as Paper 96-3161 at the AIAA/ASME/SAE/ASEE 32nd Joint Propulsion Conference, Lake Buena Vista, FL, July 1–3, 1996; received May 5, 1997; revision received May 15, 1998; accepted for publication Oct. 21, 1998.

*Graduate Student, Department of Mechanical Engineering; currently Senior Engineer, Pratt and Whitney Aircraft, United Technologies Corporation, East Hartford, CT 06108.

†Professor, Department of Mechanical Engineering; currently Professor, Department of Mechanical Engineering, Michigan State University, 2542 Engineering Building, East Lansing, MI 48824-1226. Associate Fellow AIAA.

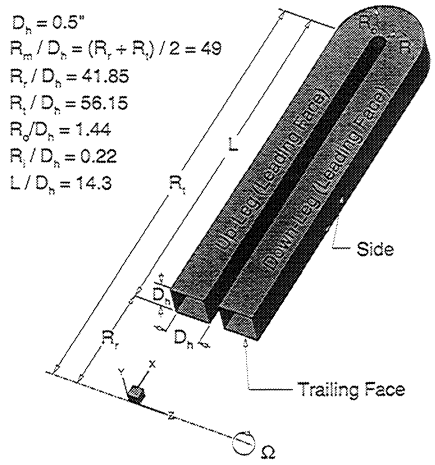

Fig. 1 Schematic of problem studied.

rate. The second key result is that rotation can also induce streamwise flow reversal or separation. This phenomenon is a consequence of centrifugal buoyancy created by the centripetal force coupled with density gradients produced by wall heat transfer. For radially outward flow, centrifugal buoyancy tends to decelerate the coolant near the wall, where the density is lower because of heat transfer. This deceleration is especially severe for the leading face because the thermal boundary layer at that location is the thickest. Thus, if there is flow reversal, it takes place on the leading face. For radially inward flow, centrifugal buoyancy accelerates instead of decelerates the lower density fluid. In this case, centrifugal buoyancy actually assists in increasing heat transfer rate. The third key result is that for a rotating duct of given geometry and radial position from the axis of rotation, heat transfer depends only on the Reynolds number, the Prandtl number, the rotation number, and the coolant-to-wall temperature ratio. On this last result, it is interesting to note that the Mach number was not included as a parameter that must be specified, even though it is clearly present in the dimensional analysis of the problem.

Mathematical studies of rotating ducts have been reported by a number of investigators.[16–26] The focus of these studies has been on the following. First, to demonstrate that simulations can predict the correct qualitative physics such as the secondary flows set up by the Coriolis force; changes in the number of vortices in the secondary flow as the rotation number increases, e.g., from two to four; and flow reversal caused by centrifugal buoyancy. Second, to develop better physical models and numerical algorithms to improve quantitative predictions. In terms of physical models, Tse et al.[26] clearly demonstrated the need to account for compressibility (see Ref. 27), and the need to use a low-Reynolds number turbulence model for the near-wall region; i.e., wall functions may be inadequate. However, what is the best turbulence model or how turbulence should be modified for rotation is still unclear. And finally, to show how detailed fluid mechanics affect the local heat transfer as a function of the Reynolds and rotation numbers. In this endeavor, the work of Prakash and Zerkle,[21] Tekriwal,[23] Tolpadi,[24] and Tse et al.[26] are particularly noteworthy, because of their relevance to blade cooling.

At this point, it is interesting to note that all studies reported so far, experimental and mathematical, do not fix the Mach number at the inlet when parametric studies were performed. In fact, the inlet Mach number was always allowed to float arbitrarily, so that the rotational speed of the duct is falsely low (presumably so that the experimental rig can reproduce it, though real gas turbines clearly rotate much faster). Later in this paper, the important role played by Mach numbers in specifying the rotational speed for a given Reynolds number and rotation number will be shown.

Accordingly, the objective of this study is to compute the flow and heat transfer in a rotating duct in which the inlet Mach number is an additional parameter that must be specified and held constant when other parameters are varied. More specifically, the objective is to show the consequences of not specifying the inlet Mach number and to investigate the effects of Reynolds number ($Re = 2.5 \times 10^4$ and 5×10^4) and rotation number ($Ro = 0.0$, 0.24, and 0.48) on the flow and heat transfer in a rotating duct in which the inlet Mach number is held constant. This objective is to be accomplished by performing a series of one- and three-dimensional analyses. For both one- and three-dimensional analyses, compressibility induced by rotation will be accounted for. In the three-dimensional analyses, a low Reynolds number turbulence model, which allows integration to the wall, will be used; i.e., wall functions will not be used. The duct to be studied will have a square cross section and a tightly wound 180-deg bend typical of blade coolant passages. Ribs will not be considered; i.e., the duct will have smooth walls, because they further complicate an already complex flowfield, making it difficult to isolate the salient physics associated with secondary flows from Coriolis and reversed flows from centrifugal buoyancy.

The remainder of this paper is organized as follows. First, the geometry and operating parameters associated with the rotating duct investigated are described. Afterward, the formulation and the numerical method of solution are given. This is then followed by results from the one- and three-dimensional computations.

Description of Problem

A schematic diagram of the problem investigated is shown in Fig. 1. Basically, it involves coolant flow (air) in a U-shaped duct of square cross section with smooth walls that are made up of two straight sections and a 180-deg bend. The geometry of the straight section is the same as that reported in Wagner et al.[1,2] The geometry of the bend is somewhat different, and is taken from the current experimental setup at United Technologies Research Center.‡ The dimensions of the duct are as follows. The duct hydraulic diameter is $D_h = 1.27$ cm (0.5 in.). The radial position of the duct relative to the axis of rotation is given by $R_r/D_h = 41.85$ and $R_t/D_h = 56.15$, so that the mean radius is $R_m/D_h = (R_r + R_t)/2D_h = 49$. The length of the duct's straight section is $L/D_h = 14.3$. The curvature of the 180-deg bend is given by $R_i/D_h = 0.22$ and $R_o/D_h = 1.44$.

For this problem, two Reynolds numbers ($Re = 2.5 \times 10^4$ and 5.0×10^4) and three rotation numbers ($Ro = 0.0$, 0.24, and 0.48) were investigated. All other parameters were kept constant as follows. The four walls of the duct were maintained at a temperature of $T_w = 344.83$ K. The coolant temperature at the inlet was uniform at $T_i = 300$ K. This gives an inlet density ratio ($\Delta\rho/\rho$) of 0.13. The velocity profile at the duct inlet was nonuniform because of the extensive flow passages upstream. Because fully developed velocity profiles do not exist for compressible flows, the velocity profile used is the one at the exit of a nonrotating straight duct of length $150D_h$ with adiabatic walls, and the same cross section and flow conditions as the U-duct. To complete specification of this problem, either the inlet pressure or the inlet Mach number must be imposed. Here, the inlet Mach number is imposed at $M_i = 0.05$, which gives the following rotational speeds: 3132 rpm for $Ro = 0.24$, and 6265 rpm for $Ro = 0.48$.

Problem Formulation

The governing equations for this problem were taken to be the ensemble-averaged conservation equations of mass (continuity), momentum (compressible Navier–Stokes), and total energy, closed by a low Reynolds number k-ω/shear stress transport turbulence model,[28–30] which can be integrated all the way to the wall. This model was selected because it satisfies many constraints required of turbulence models, such as as-

‡Wagner, J. H., and Steuber, G. D., private communication, United Technologies Research Center, East Hartford, CT, 1994.

ymptotic consistency near walls without the need for ad hoc corrections. Also, this model has been shown to give reasonable results for subsonic flows with adverse pressure gradients, separation, and streamline curvature.[30] In the governing equations, the coolant air is assumed to be a thermally and calorically perfect gas with a constant Prandtl number in which thermal conductivity can be computed by using the Sutherland's model.

Because the ensemble-averaged flow variables are steady with respect to the duct, the governing equations were written in a coordinate system, $x-y-z-t$, that rotates with the duct. If z coincides with the axis of rotation, and x is always along the duct, then the ensemble-averaged conservation equations become (see Ref. 31 for derivation):

$$\frac{\partial \rho}{\partial t} + \frac{\partial \rho u}{\partial x} + \frac{\partial \rho v}{\partial y} + \frac{\partial \rho w}{\partial z} = 0 \tag{1a}$$

$$\frac{\partial}{\partial t}\begin{bmatrix}\rho u\\ \rho v\\ \rho w\end{bmatrix} + \frac{\partial}{\partial x}\begin{bmatrix}\rho uu\\ \rho vu\\ \rho wu\end{bmatrix} + \frac{\partial}{\partial y}\begin{bmatrix}\rho uv\\ \rho vv\\ \rho wv\end{bmatrix} + \frac{\partial}{\partial z}\begin{bmatrix}\rho uw\\ \rho vw\\ \rho ww\end{bmatrix} = \frac{\partial}{\partial x}\begin{bmatrix}P^* + \tau_{xx}\\ \tau_{yx}\\ \tau_{zx}\end{bmatrix} + \frac{\partial}{\partial y}\begin{bmatrix}\tau_{xy}\\ P^* + \tau_{yy}\\ \tau_{zy}\end{bmatrix} + \frac{\partial}{\partial z}\begin{bmatrix}\tau_{xz}\\ \tau_{yz}\\ P^* + \tau_{zz}\end{bmatrix} + \phi \tag{1b}$$

$$\frac{\partial e}{\partial t} + \frac{\partial}{\partial x}(e + P^*)u + \frac{\partial}{\partial y}(e + P^*)v + \frac{\partial}{\partial z}(e + P^*)w = \frac{\partial}{\partial x}(\tau_{xx}u + \tau_{xy}v + \tau_{xz}w - q_x) + \frac{\partial}{\partial y}(\tau_{yx}u + \tau_{yy}v + \tau_{yz}w - q_y) + \frac{\partial}{\partial z}(\tau_{zx}u + \tau_{zy}v + \tau_{zz}w - q_z) + \phi_e \tag{1c}$$

where

$$P^* = P + \frac{2}{3}\rho k \tag{1d}$$

$$\phi = \begin{bmatrix}\phi_x\\ \phi_y\\ \phi_z\end{bmatrix} = \begin{bmatrix}\rho\Omega^2 x\\ \rho\Omega^2 y\\ 0\end{bmatrix} + \begin{bmatrix}2\rho v\Omega\\ -2\rho u\Omega\\ 0\end{bmatrix} \tag{1e}$$

$$\phi_e = \phi_x u + \phi_y v + \phi_z w \tag{1f}$$

In the preceding equations, τ_{ij} is the effective shear stress, P is pressure, e is mechanical plus thermal energy per unit volume, and q_i is the effective conduction in the ith direction. Note that the first and second terms on the right-hand side of Eq. (1e) represent the centripetal and the Coriolis force, respectively, which appear in the momentum and energy equations [Eqs. (1b) and (1c)].

The boundary and initial conditions for Eq. (1) and turbulence model are as follows. At the duct inlet, the velocity and temperature profiles as well as the turbulence quantities (k and ω) were specified. Pressure was extrapolated. At the duct exit, an average back pressure was imposed, but the pressure gradients in the two spanwise directions were extrapolated. This is important because secondary flows induced by the Coriolis and centripetal forces caused considerable pressure variation in the spanwise directions, so that forcing a constant pressure is incorrect. All other variables were extrapolated. At the four walls of the duct, the no-slip and constant temperature conditions were imposed. The turbulent kinetic energy (k) was set to zero. The dissipation rate per k, i.e., ω, was set to $100(\partial U/\partial n)_w$ (where U is velocity tangent to wall, and n is normal to wall), as proposed by Wilcox[28,30] for hydraulically smooth surfaces. A check, however, was imposed to ensure that the maximum value of ω was less than $60\mu/(\beta\rho Re\Delta n^2)$, as suggested by Mentor,[29] where $\beta = 3/40$ and Δn is the normal distance from the wall of the first cell.

The initial conditions used were the solutions of the steady, one-dimensional, inviscid form of Eq. (1), i.e.,

$$\frac{\partial \rho u}{\partial x} = 0, \quad \frac{\partial \rho u^2}{\partial x} = -\frac{\partial P}{\partial x} + \rho\Omega^2 x, \quad \frac{\partial \rho u H}{\partial x} = \rho u\Omega^2 x \tag{2}$$

where H is specific enthalpy. The three equations in Eq. (2) can easily be combined into the following single ordinary differential equation by using the ideal gas relations:

$$\left(\bar{R}T - \frac{c^2}{\rho^2}\right)\frac{d\rho}{dx} = \rho\Omega^2 x\left(1 - \frac{\bar{R}}{C_p}\right) \tag{3}$$

where C_p is the constant pressure specific heat, $c = \rho u$ is a constant, and

$$\frac{T}{T_i} = 1 + \frac{\Omega^2}{C_p T_i}\frac{x^2 - R_r^2}{2} \tag{4a}$$

It turns out that the solution of Eqs. (3) and (4a) is equivalent to combining the isentropic relations with Eq. (4a), i.e.,

$$\frac{\rho}{\rho_i} = \left(\frac{T}{T_i}\right)^{1/(\gamma-1)}, \quad \frac{P}{P_i} = \left(\frac{T}{T_i}\right)^{\gamma/(\gamma-1)}, \quad \frac{u}{u_i} = \frac{\rho_i}{\rho} = \left(\frac{T}{T_i}\right)^{-1/(\gamma-1)} \tag{4b}$$

By using Eq. (4) as the initial condition, the convergence rate to steady state was accelerated by a factor of more than 2.

Numerical Method of Solution

Solutions to the governing equations described in the previous section were obtained by using a modified version of the CFL3D[32,33] code, developed at NASA Langley Research Center. Modifications that were made include adding source terms that represent centripetal and Coriolis forces in the momentum and energy equations [see Eqs. (1b) and (1c)], so that steady-state solutions in a rotating frame of reference can be obtained; initial conditions based on Eq. (3); and an outflow boundary condition that enforce an average back pressure but allow spanwise gradients to be retained.

The CFL3D code is based on a cell-center finite volume method. All inviscid terms were approximated by a second-order flux-difference splitting of Roe.[34,35] Flux difference was used to minimize errors from numerical diffusion. Because only steady-state solutions were of interest, time derivatives were approximated by the Euler implicit formula. The system of nonlinear equations that resulted from the aforementioned approximations to the space and time derivatives were analyzed by using a diagonalized alternating-direction scheme,[36] with local time stepping (local Courant number always set to unity) and three-level V-cycle multigrid.[37,38]

The domain of the problem was replaced by a single-block grid system that was assembled by patching together three blocks of H–H structured grids with C^2 continuity at all block interfaces (see Fig. 2). For this grid system, the total number of grid points in the streamwise direction from duct inlet to outlet is 257. The number of grid points in the cross-stream plane is 65 × 65. The number and distribution of the grid points were obtained by using a very stringent set of rules of thumb, established by developers of numerical methods and turbulence models to ensure accuracy. These rules include having at least five grid points within a y^+ of 5, and having grid spacings next to walls kept constant for at least three grid points to resolve turbulent boundary layers. Other rules include orthogonality, smoothness, aligning grid with flow direction as much as possible, and keeping grid aspect ratio near unity in

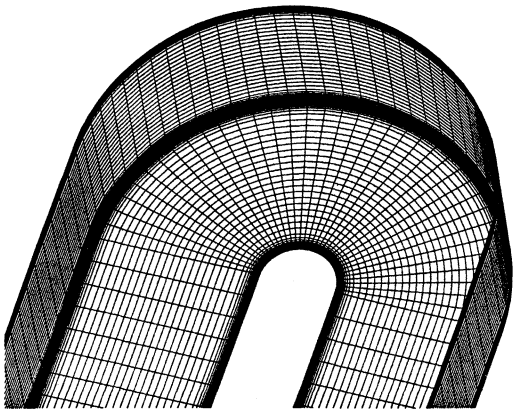

Fig. 2 Grid system used.

regions with recirculating flow. For further details on rules of thumb, see Ref. 39. As a further test, the aforementioned grid system was refined by a factor of 25% in each direction. This grid independence study showed the predicted surface heat transfer coefficient to vary by less than 3%.

On a Cray C-90 computer, where all computations were performed, the memory and CPU time requirements for each run are 55 MW and 16 h. The CPU time given is for a converged steady-state solution that typically involved 4000 iterations. A solution is said to be converged when all of the following are satisfied: 1) residual drops at least three orders of magnitude; 2) the second norm of the residual is less than 10^{-13}; 3) the mass flow rate at each cross section along the duct is within 1% of each other, which implies that unsteadiness in the continuity equation from pressure waves is minimal; and 4) the averaged heat transfer coefficient at each cross-stream plane varied by less than 1% for at least 500 iterations.

Results

This section presents the results of this study in two parts. In the first part, the analysis is one-dimensional with focus on the role of the inlet Mach number on duct rotational speed. In the second part, the analysis is three-dimensional with focus on the effects of Reynolds and rotation numbers on the multidimensional flow and heat transfer.

One-Dimensional Computations

Because the most important effect of rotation is centripetal acceleration, which acts only in the radial direction, a one-dimensional analysis is used to understand the role of the inlet Mach number on duct rotational speed. Thus, consider a one-dimensional analysis of a radially outward flow through a rotating duct, namely, the up-leg part of the U-duct shown in Fig. 1. If this one-dimensional flow is inviscid, adiabatic, and steady with respect to the rotating duct, then the governing equations are given by Eq. (2) with the solution given by Eq. (4). The pressure, temperature, density, and velocity along the duct were computed by using Eq. (4) for $Re = 2.5 \times 10^4$, $Ro = 0.24$, and four different inlet Mach numbers, $M_i = 0.0089$, 0.05, 0.1, and 0.2 (because for a given Re and Ro, an infinite number of M_i are possible). From this computation, the following observations can be made.

First, for a given Re and Ro, if the inlet Mach number (M_i) is low, then the rotational speed (Ω) is low. For example, the rotational speeds corresponding to $M_i = 0.0089$, 0.05, 0.1, and 0.2 are, respectively, Ω = 560, 3133, 6,66, and 12,532 rpm. Second, rotational speed has a very strong influence on the distributions of P, T, ρ, and u along the duct. For example, when $M_i = 0.0089$, so that Ω = 560 rpm, P, T, ρ, and u are essentially constant along the entire duct because the centripetal force is small. But when $M_i = 0.2$, so that Ω = 12,532 rpm, P, T, ρ, and u vary appreciably along the duct. For this latter case, pressure increases by a factor of 6 along the duct, temperature by a factor of about 1.6, and density by a factor of about 3.5. Because ρu = const, an increase in density causes a corresponding decrease in velocity.

There are a number of important consequences from large gradients of pressure, temperature, density, and velocity that result from high rotational speeds. First, the higher the gradient in pressure, the greater the centrifugal buoyancy, and hence, the tendency to have reverse flow in the streamwise direction next to the leading face when the Re is low. Second, because temperature increases with x from compression, the gas temperature could exceed the wall temperature. This imposes an upper limit on the coolant temperature at the duct inlet. Third, because density increases with x, so that radial velocity decreases with x for radially outward flow, velocity could actually approach zero. This also must be considered in the design of the coolant passage.

At this point, note that all studies reported so far on rotating ducts investigated cases in which pressure, temperature, density, and streamwise velocity do not vary appreciably along the duct because the rotational speed was always low. The thinking was that the Re and Ro were adequate in completely describing the physics associated with rotation for a given duct geometry, radial distance from the axis of rotation, coolant type, and coolant-to-wall temperature. This would be true if Re and Ro are both nearly constant along the duct. Because ρu is a constant for a constant-area duct, Re is nearly constant if μ is a weak function of temperature. But Eq. (4) shows that the local Ro given by

$$\frac{\Omega D_h}{u} = \frac{\Omega D_h}{u_i}\left(\frac{T}{T_i}\right)^{1/(\gamma-1)} = \frac{\Omega D_h}{u_i}\left(1_i + \frac{\Omega^2}{C_p T_i}\frac{x^2 - R_r^2}{2}\right)^{1/(\gamma-1)} \tag{5}$$

can vary appreciably along the duct. This gradient in Ro depends on Ω. This shows that studies based on low Ω cannot readily be extrapolated to real engine conditions, which typically involve high Ω, because the correct gradient in Ro was not captured. Thus, when studying compressible flows in rotating ducts, the rotation number by itself is inadequate in quantifying the physics associated with rotation. A parameter such as Eq. (5) may be more meaningful.

Three-Dimensional Computations

For the three-dimensional computations, the focus is on understanding the nature of the flow and heat transfer in the U-duct depicted in Fig. 1 in which centripetal, Coriolis, and centrifugal buoyancy are all accounted for. Computations were carried out for two Reynolds numbers (2.5×10^4 and 5×10^4) and three rotation numbers (0, 0.24, and 0.48). The computed results are given in Figs. 3–6.

Nature of Fluid Flow

The flowfield induced by rotation with a coolant-to-wall temperature less than unity can be inferred from Figs. 3 and 4. Figure 3 gives the velocity vectors in several planes between the leading and trailing faces around the bend for $Re = 2.5 \times 10^4$ and Ro = 0.0, 0.24, and 0.48. Figure 4 gives the velocity vectors in the cross-stream plane at 13 streamwise locations along the U-duct from inlet to exit for the case with $Re = 2.5 \times 10^4$ and $Ro = 0.24$.

When Ro = 0, i.e., nonrotating, the computed velocity field in the U-duct is as follows. In the up-leg part, the velocity profile has a maximum at about the center of the duct cross-section. The expected four-corner vortices were not predicted because the turbulence model employed cannot account for anisotropic effects. However, the expected pair of symmetric secondary flows (Dean type) around the bend was predicted. Also, a large streamwise separated region was found to form on the convex side of the bend about the center plane, but not

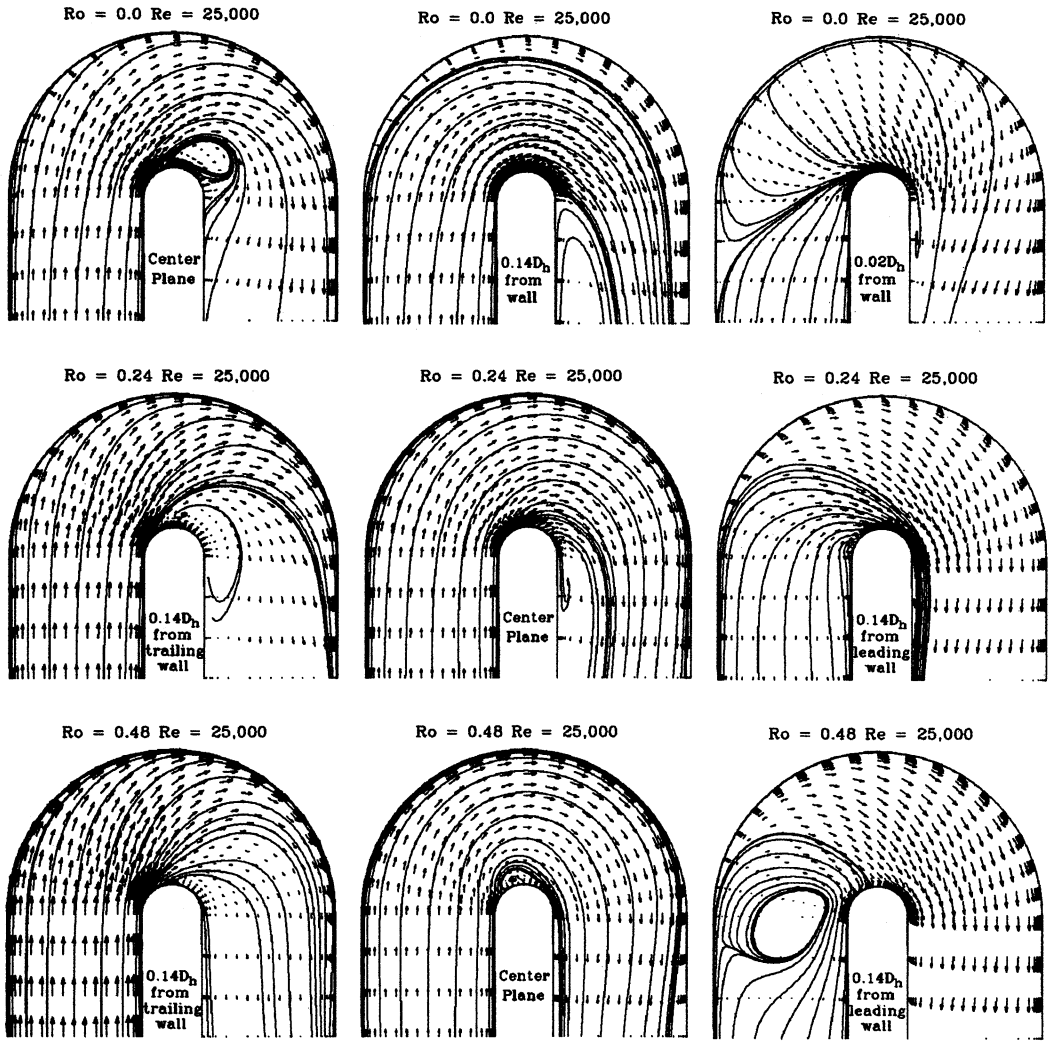

Fig. 3 Velocity vectors at three planes between the leading and trailing faces around the bend for $Re = 2.5 \times 10^4$ and $Ro = 0$, 0.24, and 0.48.

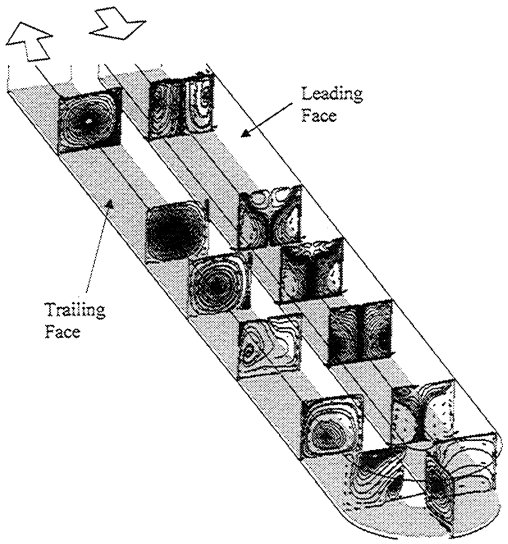

Fig. 4 Velocity vectors at 13 cross-stream planes along the U-duct for $Re = 2.5 \times 10^4$

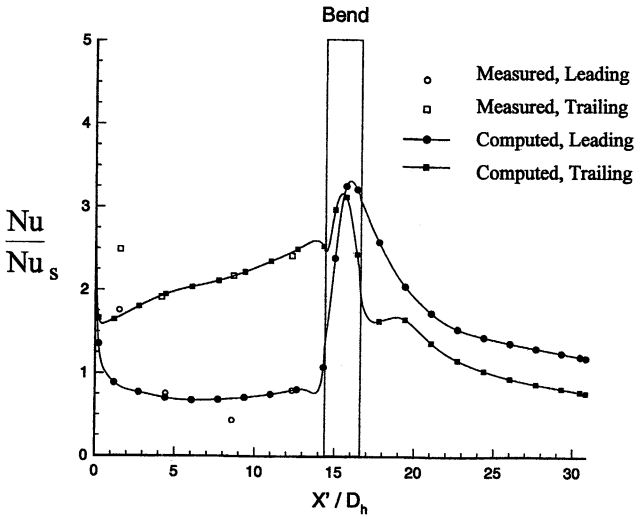

Fig. 5 Computed and measured average Nusselt number along leading and trailing faces for $Re = 2.5 \times 10^4$ and $Ro = 0.24$.

on the concave side (Fig. 3). Just downstream of the bend in the down-leg part, two more streamwise separated regions form, one on the leading face and another on the trailing face (Fig. 3). This coupled with Dean-type secondary flows shifted the peak streamwise velocity toward the outer side wall in the down-leg part.

Rotation affects the flow just described in an appreciable way. Some observations are as follows. The first observation is that with rotation, there is flow reversal in the streamwise direction on the leading face in the up-leg part. The reason for the reverse flow is centrifugal buoyancy, which decelerates fluid next to the wall because they have lower density from wall heating. The flow reverses on the leading face because

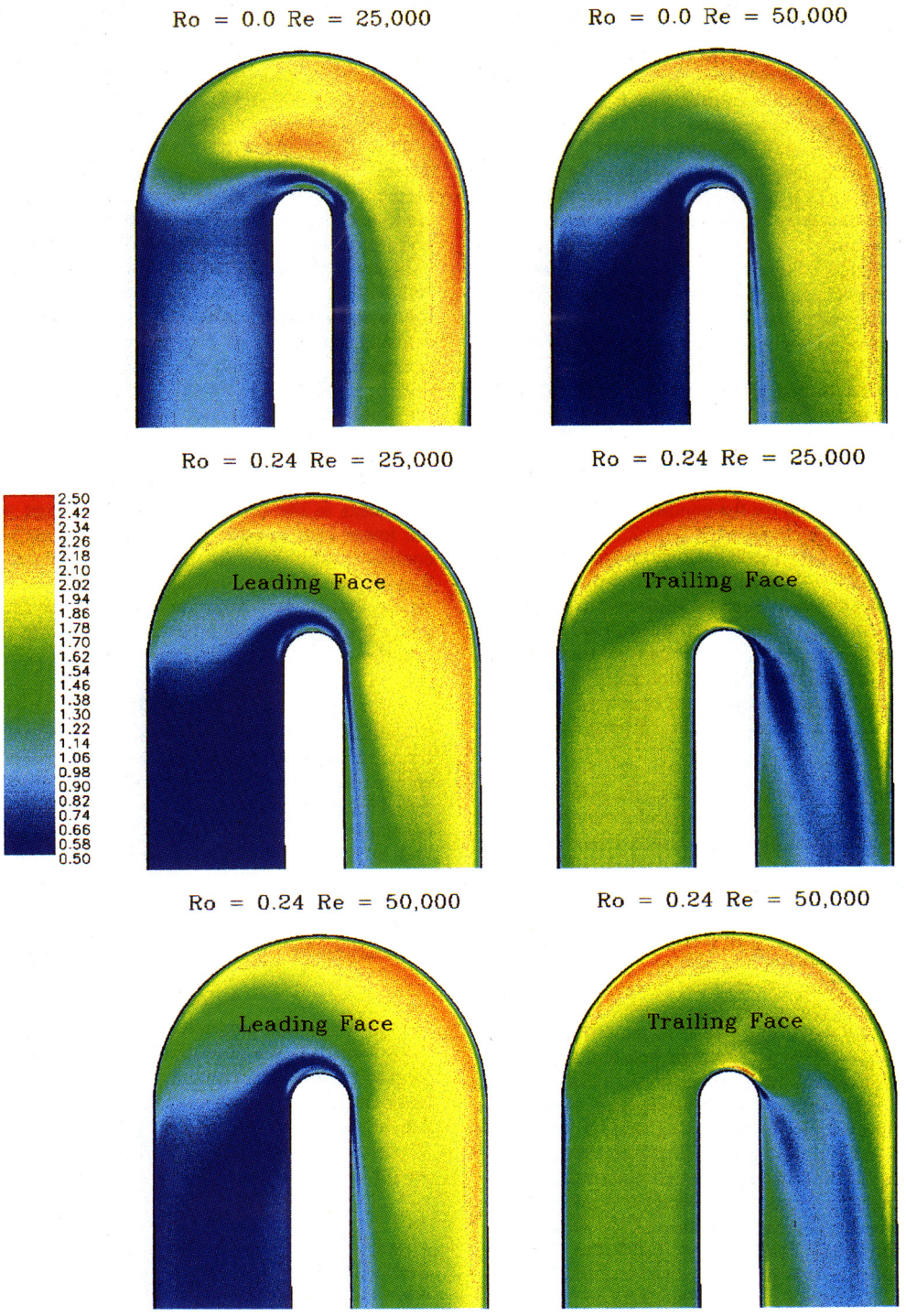

Fig. 6 Nusselt number contours on the leading and trailing faces for $Re = 2.5 \times 10^4$ and 5×10^4 at $Ro = 0.24$.

density is lowest there as a result of secondary flows from the Coriolis force. For the conditions of the present study, the size of the reverse flow region is quite appreciable when $Ro = 0.48$. This reverse flow on the leading face causes flow on the trailing face to be accelerated to satisfy continuity.

The second observation is that rotation causes the formation of many secondary flows. The formation of two symmetric counter-rotating secondary flows by Coriolis is well known. Not so well known is the formation of additional vortices and their causes. Figure 4 shows the number of secondary flows to increase from two to four, and then to six, with new ones all formed next to the leading face. The additional secondary flows formed because once the flow reversed in direction because of centrifugal buoyancy, it is flowing radially inward instead of radially outward. With radially inward flow, the secondary flows formed by Coriolis force have an opposite sense of rotation. Also, with radially inward flow, centrifugal buoyancy accelerates instead of decelerates the lower density fluid. Even without flow reversal, Coriolis-induced secondary flows can cause additional vortices to form next to the leading face because of the highly decelerated flow there. The formation of up to four secondary flows (but not six) was reported in Ref. 19. However, the reason for their formation was not advanced.

The third observation is that as the flow approaches the 180-deg bend, it is strongly affected by the Dean-type secondary flows created there. However, unlike the nonrotating case, the two secondary flows around the bend are not symmetric (Fig. 4). The one next to the leading face is much larger than the one next to the trailing face. There are two reasons for this asymmetry. The first reason is that the secondary flows set up

by the Coriolis force in the up-leg part of the duct reinforces the Dean-type secondary flow next to the leading face, but weaken the one next to the trailing face. The second reason is that centrifugal buoyancy near the leading face is much higher than that on the trailing face because the fluid there is hotter. This higher centrifugal buoyancy also reinforces the Dean-type secondary flow next to the leading face more so than the one next to the trailing face. The net effect of the asymmetry on the secondary flows is that they induce a motion on each other as they flow downstream.

The fourth observation is that there is a large streamwise separation bubble around and downstream of the bend next to the trailing face, but a very small one next to the leading face (Fig. 3). This is because of the asymmetry of secondary flows in the bend.

The fifth observation is that after the bend, only one secondary flow dominates, this is the one that flows from the concave to the convex side along the leading face. This secondary flow was reinforced in the down-leg part by the Coriolis force.

The sixth observation is that for the conditions of the present study, the flow features associated with $Re = 2.5 \times 10^4$ and 5×10^4 at a given Ro are very similar. However, the flow features associated with $Ro = 0.24$ and $Ro = 0.48$ at a given Re are very different. This difference can be attributed to the small temperature difference imposed between the wall and coolant temperatures. When $Ro = 0.24$, the coolant temperature is lower than the wall temperature throughout the U-duct. But, when $Ro = 0.48$, the coolant temperature exceeded the wall temperature before the coolant reaches the 180-deg bend.

Heat Transfer Characteristics

In this section, the heat transfer characteristics in the U-duct are described with focus on effects from fluid mechanics. The heat transfer results are given in Figs. 5 and 6. Figure 5 gives the averaged Nusselt number on the leading and trailing faces, where the average is along the perimeter of the cross-stream plane. Figure 5 also gives the measured quantities from Wagner et al.[1] Figure 6 gives normalized Nusselt number (Nu/Nu_s) contours on the leading and trailing faces.

From Fig. 5, the following observations can be made about the heat transfer rate in the up-leg part of the U-duct. First, the Nusselt number on the leading face is much lower than that on the trailing face. This is expected because secondary flows created by the Coriolis force moves cooler fluid near the center of the duct cross-section to the trailing face, so that the thermal boundary layer starts on the trailing face, grows along the two side walls, and ends at the leading face. Second, the Nusselt number on the trailing face rises continuously, except near the duct entrance. The rise after the initial decrease on the trailing face is caused by the formation of the first pair of secondary flows from the Coriolis force. Third, the variation of the Nusselt number on the leading face is less dramatic; it initially decreases, then rises slowly. The decrease is caused by thermal boundary-layer growth and formation of the first pair of secondary flows. The rise is a result of the formation of the second and third pairs of secondary flows, which circulate lower temperature fluid about the leading face.

Figure 5 shows the following about the heat transfer characteristics in the bend and the down-leg part of the U-duct. First, the Nusselt number on both the leading and trailing faces rise around the bend, with the rise on the leading face being more dramatic, because the boundary layer is fuller there and it receives more cooler fluid from near the center of the duct cross section. In the down-leg part of the duct, the Nusselt number on the leading face becomes higher than that on the trailing face. The reason for this is that when the flow is radially inward, Coriolis force reverses direction when compared with the radially outward flow, and causes cooler fluid to first approach the leading face instead of the trailing face.

Note that Fig. 5 also gives experimentally measured values of the averaged Nusselt number from Wagner et al.[1] Comparing the computed with the measured results shows good agreement, except near the duct entrance for the trailing face and the minimum value for the leading face. The difference near the duct entrance is because of differences in the inflow velocity and turbulence profiles, the effects of which diminish with x. The difference for the minimum Nusselt number on the leading face is attributed to inadequacies of the turbulence model. Although there are some differences between the computed and the measured results, the generally good agreement gives confidence to the validity of the computations.

Figure 6 shows the Nusselt number contours on the trailing and leading faces normalized by Nu_s. From this figure, the following observations can be made. First, when $Ro = 0$, increasing Re decreases Nu/Nu_s, which is consistent with experimental observation. But, when $Ro = 0.24$, increasing Re decreases Nu/Nu_s, everywhere except on the trailing face of the down-leg part. Second, when $Ro = 0$, heat transfer is highest in the bend next to the downstream side of the concave wall. This is because the flow from the up-leg part impinges there. When $Ro = 0.24$, the highest heat transfer is also in the bend next to the concave wall, but is more upstream. Third, the lower heat transfer regions just downstream of the bend correlate well with the observed separated regions there. Fourth, when there is rotation, the heat transfer rate is higher on the trailing face from the up-leg part to the bend, but generally lower elsewhere when compared with the case without rotation.

Summary

Computations were performed to examine the fluid mechanics and heat transfer in a U-duct. The one-dimensional analysis showed that for a given Re and Ro, many rotational speeds are possible, giving rise to widely different flows. Also, along a constant-area duct, the rotation number can vary appreciably and is a strong function of the rotational speed. The three-dimensional analysis showed the nature of the flow in rotating U-ducts caused by Coriolis, centrifugal buoyancy, and bend, as well as how this flow affects heat transfer. The computed results compared well with available experimental data.

Acknowledgments

This work was supported by NASA Grant NAG 3-1727, from NASA Lewis Research Center under the Smart Green Engine Project. The computer time was provided by NASA's National Aerospace Simulation facility. The authors are grateful for this support. The first author also thanks Kestutis C. Civinskas and David L. Rigby of NASA Lewis Research Center for helpful discussions.

References

[1]Wagner, J. H., Johnson, B. V., and Hajek, T. J., "Heat Transfer in Rotating Passages with Smooth Walls and Radial Outward Flow," *Journal of Turbomachinery*, Vol. 113, No. 1, 1991, pp. 42–51.

[2]Wagner, J. H., Johnson, B. V., and Kopper, F. C., "Heat Transfer in Rotating Serpentine Passages with Smooth Walls," *Journal of Turbomachinery*, Vol. 113, No. 3, 1991, pp. 321–330.

[3]Wagner, J. H., Johnson, B. V., Graziani, R. A., and Yeh, F. C., "Heat Transfer in Rotating Serpentine Passages with Trips Normal to the Flow," *Journal of Turbomachinery*, Vol. 114, No. 4, 1992, pp. 847–857.

[4]Johnson, B. V., Wagner, J. H., Steuber, G. D., and Yeh, F. C., "Heat Transfer in Rotating Serpentine Passages with Selected Model Orientations for Smooth or Skewed Trip Walls," *Journal of Turbomachinery*, Vol. 116, No. 4, 1994, pp. 738–744.

[5]Morris, W. D., and Ghavami-Nasr, G., "Heat Transfer Measurements in Rectangular Channels with Orthogonal Model Rotation," *Journal of Turbomachinery*, Vol. 113, No. 3, 1991, pp. 339–345.

[6]Morris, W. D., and Salemi, R., "An Attempt to Uncouple the Effects of Coriolis and Buoyancy Forces Experimentally on Heat Transfer in Smooth Circular Tubes That Rotate in the Orthogonal Mode," *Journal of Turbomachinery*, Vol. 114, No. 4, 1992, pp. 858–864.

[7]Han, J. C., Zhang, Y. M., and Kalkuehler, K., "Uneven Wall Temperature Effect on Local Heat Transfer in a Rotating Two-Pass Square

Channel with Smooth Walls," *Journal of Turbomachinery*, Vol. 115, No. 4, 1993, pp. 912, 920.

[8]Han, J. C., Zhang, Y. M., and Lee, C. P., "Influence of Surface Heating Condition on Local Heat Transfer in a Rotating Square Channel with Smooth Walls and Radially Outward Flow," *Journal of Turbomachinery*, Vol. 116, No. 1, 1994, pp. 149–158.

[9]Zhang, Y. M., Han, J. C., Parsons, J. A., and Lee, C. P., "Surface Heating Effect on Local Heat Transfer in a Rotating Two-Pass Square Channel with 60 Deg Angled Rib Turbulators," *Journal of Turbomachinery*, Vol. 117, No. 2, 1995, pp. 272–280.

[10]Soong, C. Y., Lin, S. T., and Hwang, G. J., "An Experimental Study of Convective Heat Transfer in Radially Rotating Rectangular Ducts," *Journal of Heat Transfer*, Vol. 113, No. 3, 1991, pp. 604–611.

[11]Kuo, C. R., and Hwang, G. J., "Experimental Studies and Correlations of Radially Outward and Inward Air-Flow Heat Transfer in a Rotating Square Duct," *Journal of Heat Transfer*, Vol. 118, No. 1, 1996, pp. 23–30.

[12]Taslim, M. E., Rahman, A., and Spring, S. D., "An Experimental Investigation of Heat Transfer Coefficients in a Spanwise Rotating Channel with Two Opposite Rib-Roughened Walls," *Journal of Turbomachinery*, Vol. 113, No. 1, 1991, pp. 75–82.

[13]Taslim, M. E., Bondi, L. A., and Kercher, D. M., "An Experimental Investigation of Heat Transfer in an Orthogonally Rotating Channel Roughened with 45 Deg Criss-Cross Ribs on Two Opposite Walls," *Journal of Turbomachinery*, Vol. 113, No. 3, 1991, pp. 346–353.

[14]Zhang, N., Chiou, J., Fann, S., and Yang, W.-J., "Local Heat Transfer Distribution in a Rotating Serpentine Rib-Roughened Flow Passage," *Journal of Heat Transfer*, Vol. 115, No. 3, 1993, pp. 560–567.

[15]Tse, D. G. N., "Flow in Rotating Serpentine Coolant Passages with Skewed Trip Strips," Scientific Research Associates, Inc., R95-9089F, Glastonbury, CT, Nov. 1995.

[16]Warfield, M. J., and Lakshminarayana, B., "Computation of Rotating Turbulent Flow with an Algebraic Reynolds Stress Model," *AIAA Journal*, Vol. 25, No. 7, 1987, pp. 957–964.

[17]Galperin, B., and Kantha, L. H., "Turbulence Model for Rotating Flows," *AIAA Journal*, Vol. 27, No. 6, 1989, pp. 750–757.

[18]Yoo, G. J., So, R. M. C., and Hwang, B. C., "Calculation of Developing Turbulent Flows in a Rotating Pipe," *Journal of Turbomachinery*, Vol. 113, No. 1, 1991, pp. 34–41.

[19]Iacovides, H., and Launder, B. E., "Parametric and Numerical Study of Fully Developed Flow and Heat Transfer in Rotating Rectangular Ducts," *Journal of Turbomachinery*, Vol. 113, No. 3, 1991, pp. 331–338.

[20]Medwell, J. O., Morris, W. D., Xia, J. Y., and Taylor, C., "An Investigation of Convective Heat Transfer in a Rotating Coolant Channel," *Journal of Turbomachinery*, Vol. 113, No. 3, 1991, pp. 354–359.

[21]Prakash, C., and Zerkle, R., "Prediction of Turbulent Flow and Heat Transfer in a Radially Rotating Square Duct," *Journal of Turbomachinery*, Vol. 114, No. 4, 1992, pp. 835–846.

[22]Prakash, C., and Zerkle, R., "Prediction of Turbulent Flow and Heat Transfer in a Ribbed Rectangular Duct with and Without Rotation," *Journal of Turbomachinery*, Vol. 117, No. 2, 1995, pp. 255–264.

[23]Tekriwal, P., "Heat Transfer Predictions with Extended k-ε Turbulence Model in Radial Cooling Ducts Rotating in Orthogonal Mode," *Journal of Heat Transfer*, Vol. 116, No. 2, 1991, pp. 369–380.

[24]Tolpadi, A. K., "Calculation of Heat Transfer in a Radially Rotating Coolant Passage," AIAA Paper 94-0261, Jan. 1994.

[25]Dutta, S., Andrews, M. J., and Han, J. C., "Simulation of Turbulent Heat Transfer in a Rotating Duct," *Journal of Thermophysics and Heat Transfer*, Vol. 9, No. 2, 1994, pp. 381, 382.

[26]Tse, D. G. N., Kreskovsky, J. P., Shamroth, S. J., and McGrath, D. B., "A Combined Experimental/Computational Study of Flow in Turbine Blade Cooling Passage," NASA CR-4584, May 1994.

[27]Besserman, D. L., and Tanrikut, S., "Comparison of Heat Transfer Measurements with Computations for Turbulent Flow Around a 180 Degree Bend," American Society of Mechanical Engineers, Paper 91-GT-2, June 1991.

[28]Wilcox, D. C., "A Half Century Historical Review of the k-ω Model," AIAA Paper 91-0615, Jan. 1991.

[29]Menter, F. R., "Improved Two-Equation k-ω Turbulence Models for Aerodynamic Flows," NASA TM 103975, 1992.

[30]Wilcox, D. C., "Turbulence Modeling for CFD," DCW Industries, La Canada, CA, 1993.

[31]Steinthorsson, E., Shih, T. I-P., and Roelke, R. J., "Computations of the Three-Dimensional Flow and Heat Transfer Within a Coolant Passage of a Radial Turbine Blade," AIAA Paper 91-2238, June 1991.

[32]Thomas, J. L., Krist, S. T., and Anderson, W. K., "Navier-Stokes Computations of Vortical Flows over Low-Aspect-Ratio Wings," *AIAA Journal*, Vol. 28, No. 2, 1990, pp. 205–212.

[33]Rumsey, C. L., and Vatsa, V. N., "A Comparison of the Predictive Capabilities of Several Turbulence Models Using Upwind and Central-Difference Computer Codes," AIAA Paper 93-0192, Jan. 1993.

[34]Roe, P. L., "Approximate Riemann Solvers, Parameter Vector and Difference Schemes," *Journal of Computational Physics*, Vol. 43, Oct. 1981, pp. 357–372.

[35]Roe, P. L., "Characteristic Based Schemes for the Euler Equations," *Annual Review of Fluid Mechanics*, Vol. 18, 1986, pp. 337–365.

[36]Pulliam, W. R., and Chaussee, D. S., "A Diagonal Form of an Implicit Approximate Factorization Algorithm," *Journal of Computational Physics*, Vol. 39, 1981, pp. 347–363.

[37]Ni, R.-H., "A Multiple Grid Scheme for Solving the Euler Equations," AIAA Paper 81-1025, 1981.

[38]Anderson, W. K., Thomas, J. L., and Whitfield, D. L., "Multigrid Acceleration of the Flux-Split Euler Equations," *AIAA Journal*, Vol. 26, No. 6, 1988, pp. 649–654.

[39]Stephens, M. A., Chyu, M. K., Shih, T. I-P., and Civinskas, K. C., "Calculations and Measurements of Heat Transfer in a Square Duct with Inclined Ribs," AIAA Paper 96-3163, July 1996.